THE ELEMENTAL AND ISOTOPIC COMPOSITION OF GALACTIC COSMIC RAYS

R.A. Mewaldt
California Institute of Technology
Pasadena, California 91125
U.S.A.

1. Introduction

Galactic cosmic rays represent a directly accessible sample of matter that originates outside the solar system. The element and isotope distribution of this high-energy material is a record that was molded in the fires of nucleosynthesis in other regions of the galaxy, and imprinted by subsequent nuclear and electromagnetic processes that have altered its composition. Recently, significant new advances have been achieved in reading this record, brought about in large part by the launch of new high-resolution instrumentation for measuring the charge, mass, and energy distribution of cosmic ray nuclides. In general, the data from these new experiments are telling us what is different about this extra-solar sample.

This rapporteur paper reviews progress in this area that was reported at the 17th International Cosmic Ray Conference in Paris. In general, the sessions covered (OG H.2, H.3, 1.1, 1.2) addressed the following questions:

> What is the composition of the material that gets accelerated to be cosmic rays? In what ways is it similar to, or different from, solar system material?

In this paper I will attempt to summarize the answers that we have to these questions from the new data reported at this conference. In most cases I will stop short of interpreting the observations in terms of specific models of cosmic ray nucleosynthesis, acceleration, or propagation. Rather I will try to set the stage for other rapporteurs (including M. Cassé, S. A. Stephens, and H. J. Volk) who will deal in detail with these subjects.

Table 1 gives a breakdown of specific topics covered in these sessions, and lists the related conference papers. I will focus on those new results that in my opinion are potentially the most significant and interesting, and attempt to put them in the context of earlier work. The remainder of this paper is divided into five areas:

Elemental Composition ($1 \leq Z \leq 30$)
UH ($Z > 30$) Cosmic Rays
Cosmic Ray Clocks
Cross Sections
Cosmic Ray Isotopes

2. The Elemental Composition of $1 \leq Z \leq 30$ Nuclei

2.1 Observations: Measurements of the elemental composition of cosmic rays are, of course, critical for determining the composition of cosmic ray source material; in addition these data provide important tests of

Table 1 - Summary of Contributed Papers

Topic	Papers*
Elemental Composition (1≤Z≤30)	
Relative Abundances	H.2-1, H.3-2, 1.1-4, 1.1-6, 4-3
Energy Spectra	H.2-2, 1.1-1, 1.1-2, 1.1-3, 1.1-4, 1.1-5,1.1-6, 1.1-7
Source Composition	H.3-10, 1.1-1, 4-1, 4-2, 4-3, 4-4
UH (Z > 30) Cosmic Rays	
Observations	H.2-8, H.2-9, H.2-10
Interpretation	H.3-9, H.3-12, H.3-13, H.3-14, H.3-15, H.3-16, 4-7
Cosmic Ray Clocks	H.3-2, H.3-3, H.3-4, H.3-7, 1.2-3, 4-1
Cross Sections	H.3-6, 3.1-1, 3.1-2, 3.1-3, 3.1-5
Cosmic Ray Isotopes	
Source Composition	H.2-3, H.2-4, 1.2-2, 1.2-4, 1.2-6, 1.2-7, 4-1, 4-3
Secondary Nuclei	H.2-3, H.2-4, 1.2-1, 1.2-2, 1.2-3, 1.2-6, 4-3
Anomalous Component	1.2-1,1.2-2
Experimental Techniques	H.2-5, 1.2-8

* All paper codes refer to the OG session (OG H.2-1 is H.2-1) printed in Volume 2 of the proceedings. Footnotes in brackets refer to pre-conference references.

models of cosmic ray acceleration, propagation, and solar modulation. I will concentrate here on the question of the source composition.

Although this field is now more than 30 years old, significant new progress has recently been achieved in determining the arriving element distribution, most notably by the French-Danish experiment on HEAO-3 (HEAO3-C2 experiment). This experiment combines excellent charge resolution, energy resolution, and statistical accuracy over an extended energy region (~0.6 to ~20 GeV/nucleon). Figure 1 shows an example of the HEAO3-C2 data in the difficult region just above the Fe peak. This represents the first time Cu (nuclear charge Z=29) has been resolved, the last element with Z≤30 to be identified in the arriving cosmic rays. The Chicago group (4-2) has achieved comparable resolution with a balloon experiment covering 1.2 to 2.4 GeV/nucleon, and their results generally agree excellently with the HEAO data.

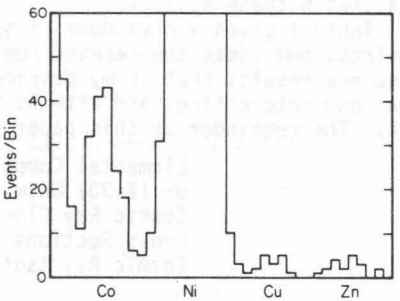

Figure 1: Charge histogram for 27≤Z≤30 nuclei with >2 GeV/nuc. from HEAO3-C2 [1]. Note resolved peaks at Co, Cu and Zn.

Previous observations have shown that the mean pathlength traversed at energies ≥1 GeV/nucleon is energy dependent, as demonstrated in Figure 2, which shows the observed energy dependence of several abundance ratios. Since the elements in the numerator are all reasonably rare in the source composition,

the energy dependence is dominated by the varying secondary contribution, fit here by a rigidity dependent pathlength $\propto R^{-0.5}$ (see also H.3-7 and 3.1-6). Source contributions are reflected by the absolute level, and also by the slope of these ratios (note that Al/Fe and Na/Fe are flatter than P/Fe or K/Fe due to the greater source abundances of Al and Na). Thus studies in this energy region can provide especially sensitive measures of the source composition. The HEAO study (H.3-10) derived source abundances for 16 elements and upper limits for several others. In addition, the Chicago (4-2) and New Hampshire (4-3) groups reported new source abundances.

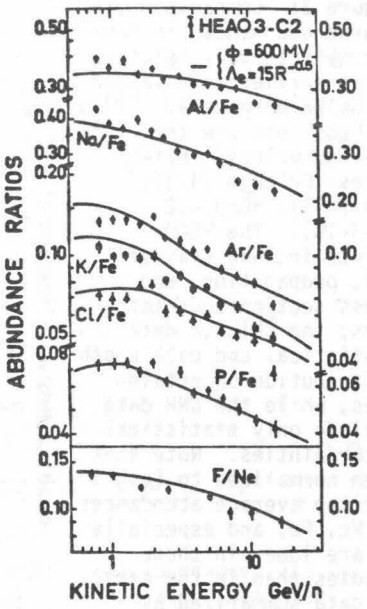

Figure 2: Energy dependence of several abundance ratios (H.2-1). The fits assume an escape length $\propto R^{-0.5}$. The scatter in the data suggests small errors in the energy interval calibration. Note, however, that the statistical errors are ~10 times smaller than earlier experiments in this region.

2.2 Energy Dependence of the Source Composition: The question of whether the source composition is energy dependent has important implications for theoretical models, including those that invoke multiple sources of cosmic rays. In (4-2) the Chicago group presented possible evidence for an energy dependent source composition based on a comparison of studies at ~200 and ~1600 MeV/nucleon. On the other hand the HEAO3-C2 group (H.3-10) concluded that their ~1 to ~15 GeV/nucleon data were consistent with an energy-independent source composition, although some elements like Si were not as well fit as others. This question is addressed in Figure 3, which compares source abundances of 10 relatively abundant nuclei as determined in four energy intervals. In general, there is reasonable agreement at most elements, and it would appear that any possible systematic energy dependence is at most 10 to 20% in magnitude. While there is a tendency for the abundances of the lighter elements (C to Si) to be greater in the ~200 MeV/nucleon Chicago data (when normalized to Fe), it was also pointed out that these low-energy source abundances are more sensitive to the details of the propagation model (4-2, 3.1-9), which may account for this trend. While further work on propagation/modulation models is clearly needed to unify the interpretation of observations made at widely separated energies, at this point it would appear that the assumption of an energy-independent source composition is reasonable.

2.3 Comparison With Solar System Abundances: It has been known for some time that the ratio of galactic cosmic ray source (GCRS) abundances to solar system abundances is organized by first ionization potential (I), or some related atomic parameter (see, e.g., [3]). Figure 4 shows

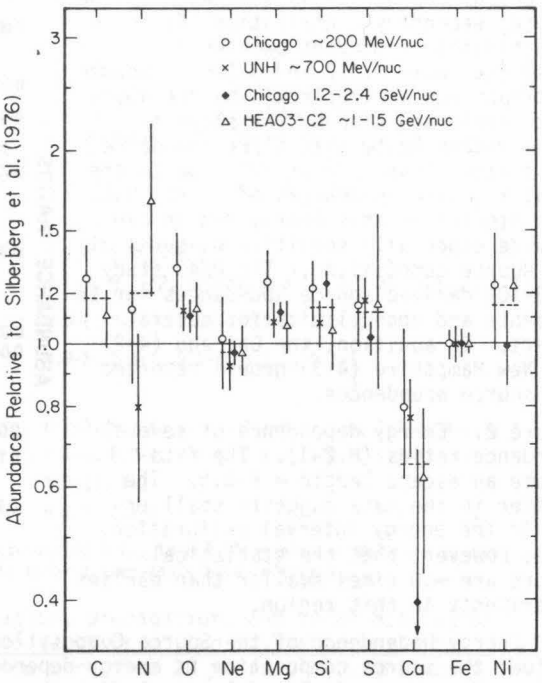

Figure 3: Comparison of source abundances in four energy intervals relative to an earlier compilation by Silberberg et al. [2]. Dashed lines are the average values. References: Chicago (4-2); UNH (4-3); HEAO3-C2 (H.3-10). The HEAO points include statistical, propagation, and cross section uncertainties; the Chicago data statistical and pathlength distribution uncertainties; while the UNH data include only statistical uncertainties. Note that when normalized to (e.g.) Si, the average abundances of Ne, Fe, and especially Ca are lower in these studies than in the earlier data summarized by Silberberg et al.

a comparison of GCRS and "local galactic" (LG, see [4]) abundances for 24 elements with $6 \leq Z \leq 42$. Recent additions to this plot include Co, Cu, and even-Z elements with $32 \leq Z \leq 42$. With the exception of Mo (Z=42), these additions fit the pattern of the earlier data.

There was some discussion at the conference over whether this comparison was best represented by an exponential dependence on I (as suggested by earlier GCR work), or by a series of two plateaus (4-4), with elements having $I \gtrsim 9$ eV depleted by a factor of ~4 (when Si ≡ 1.0), a dependence suggested earlier by solar energetic particle abundances. In the absence of a quantitative physical model for either, a comparison of Figures 4a and 4b suggests that this choice is presently determined mainly by what type of graph paper is available.

Figure 5 shows a comparison of GCRS and average solar energetic particle abundances adapted from Meyer (4-4). Note that this ratio is ~1 for at least 10 elements, suggesting that the source composition and any injection/acceleration biases must be similar, as concluded by Webber [5] on the basis of earlier data. Notable exceptions occur at C and He. Isotope studies reported at this conference (1.2-2, 4-3) find significantly lower GCR source abundances for N than the HEAO study does, suggesting that GCR N may be depleted by a factor of ~3 or more, which would make N anomalous in Figures 4 and 5 (see discussion in Section 2.4). Webber et al. (4-3) have pointed out that ^{20}Ne (as opposed to total Ne) is also underabundant in GCR's when compared to SEP's (since ~40% of GCR neon in ^{22}Ne).

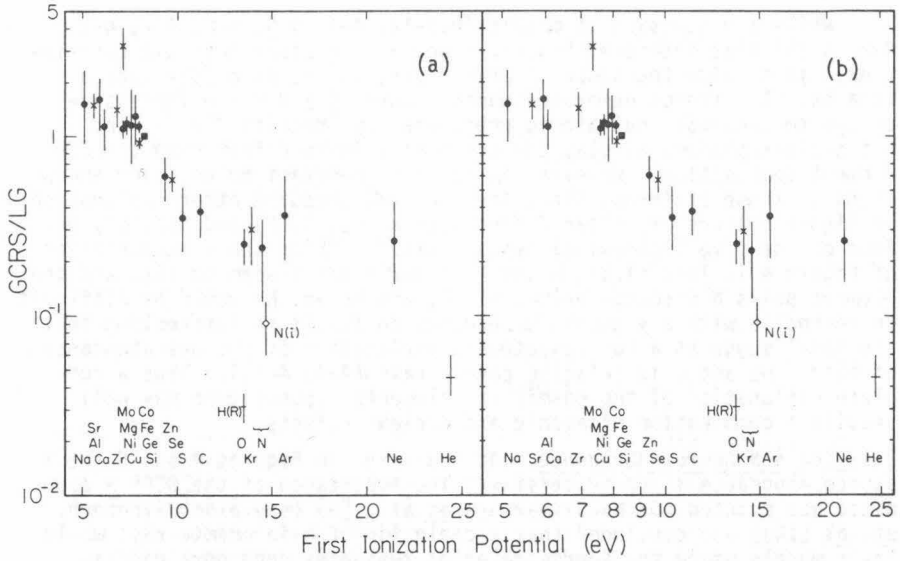

Figure 4: a) Ratio of GCRS to "local galactic" (LG) abundances vs. first ionization potential, adapted from (4-4) and (H.3-12). Data for $6 \leq Z \leq 30$ (●) are from HEAO3-C2 (H.3-10) and include both GCRS and LG uncertainties. Data for $32 \leq Z \leq 42$ (x) are from the HEAO UH experiment (H.2-8, [6], [7]) and use solar system [8] abundances for LG (with no uncertainties). H and He GCRS abundances are from [3] where H(R) assumes rigidity spectra. The nitrogen N(i) point (◇) is based on N isotope studies (see Section 2.4). b) Log-log plot of data in Fig. 4a.

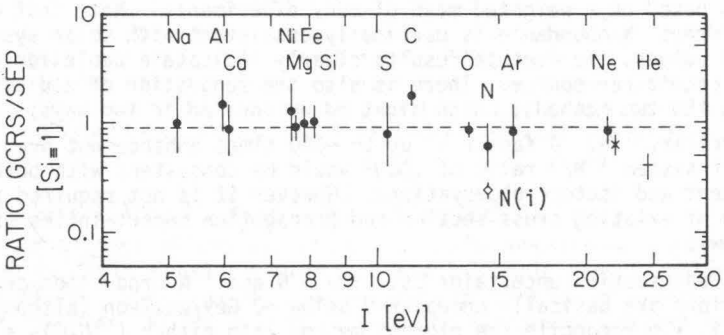

Figure 5: Ratio of GCRS to solar energetic particle (SEP) abundances adapted from (4-4). GCRS abundances (except He) are from (H.3-10), with SEP abundances from (SH 3.1-10). The N(i) point is described in Figure 4. The ^{20}Ne point (x) uses average GCRS abundances for neon (Figure 3) and $^{22}Ne/^{20}Ne$ (Figure 16). The dashed line is the mean ratio from (4-4).

While a discussion of models (H.3-12, 4-4, 4-5, 4-6, 4-7, 4-8, 4-9, 4-39) that interpret Figures 4 and 5 (and other possible correlations) is outside the scope of this paper, let me make some general remarks. The trends demonstrated in Figures 4 and 5 are impressive enough to conclude that atomic phenomena (not necessarily I), and not nuclear phenomena, play the dominant role in determining the GCR element composition. However, it is also important to note the exceptions to these patterns, since they may well require other explanations. In Figure 5 there are clear differences at He, C, N, and possibly Ne, four of the five lightest elements plotted. While the interpretation of Figure 4 is less clear, H and Mo clearly don't seem to fit, and the element pairs N (isotope value) vs. O, and He vs. Ne would be difficult to reconcile with any smooth dependence on I. It is interesting that one model suggests a nucleosynthesis explanation of the overabundance of both ^{22}Ne and C in galactic cosmic rays (4-4, 4-12). Thus a complete explanation of the cosmic ray elemental composition may well require a combination of atomic and nuclear effects.

2.4 The ^{14}N Source Abundance: As indicated in Figures 4 and 5 the N source abundance is controversial. The importance of the GCRS N abundance was pointed out by Silberberg et al. [9] (see also Hainebach et. al [10]) who concluded that a depletion of N in cosmic rays would favor models where the source material resembles supernova ejecta rather than the interstellar medium (ISM).

The N source abundance can be determined in two ways. The "element method" measures N/O and subtracts secondary N using a propagation model. Typically $(N/O)_s \simeq 0.07$ (see Tables 2 and 3). The "isotope method" measures ^{15}N/N and N/O, and then uses ^{15}N as a tracer ($^{15}N/N = 0.004 \simeq 0$ in solar system) to determine the secondary ^{14}N. Isotope results reported at this conference give $(^{14}N/O)_s \leq 0.04$ (1.2-2, [11]) and $(^{14}N/O)_s = 0.030 \pm .014$ (4-3), both considerably less than found from typical element studies.

Table 3 summarizes ^{14}N/O determinations including cosmic ray results based on a weighted mean of many experiments. Note that while the "element" N abundance is marginally consistent with solar system and ISM values, the isotope results clearly indicate a depletion of ^{14}N in the cosmic ray source. There is also the suggestion of a discrepancy between the two methods, which might be reconciled in two ways:

1) Primary ^{15}N: A factor of up to ~100 times enhancement over the solar system ^{15}N/O ratio of .0005 would be consistent with both the element and isotope observations. However it is not required in view of existing cross section and propagation uncertainties (see below).

2) Cross section uncertainties: The ^{14}N and ^{15}N production cross sections are basically unmeasured below ~2 GeV/nucleon (although see [15]). To reconcile the element method with either $(^{14}N/O)_s = 0.04$ or 0.10 requires only 12 to 16% cross section errors for N production (or for tracer used, e.g., Li, Be, B), certainly not unreasonable. For the isotope method, note that

$$\left(\frac{^{14}N}{O}\right)_s \simeq \left(\frac{^{14}N}{O}\right)_{obs.} - \left(\frac{\sigma_{14}}{\sigma_{15}}\right)\left(\frac{^{15}N}{O}\right)_{obs.} \simeq 0.13 - (0.57)(0.16) \simeq 0.04,$$

Table 2

Cosmic Ray Nitrogen Observations

Ratio	Value	References
N/O	0.29±.01	Weighted mean of experiments reporting N/O and ^{15}N/N ([12], [13], [14], [15], [11], 4-3)
^{14}N/O	0.13±.01	
^{15}N/O	0.16±.01	
^{15}N/N	0.57±.02	
^{15}N/N	0.55±.02	Add in [16], [17], [18], [19]

Table 3 - ^{14}N/O Observations

	^{14}N/O	References
Solar System		
"Sun"	0.13±.05	[20]
Photosphere	0.12±.04	[21]
Corona	0.14±.01	[22]
Solar Flares	0.12±.01	[23]
Interstellar Medium	~0.10	[24]
"Local Galactic"	0.10±.04	[4]
Cosmic Ray Source		
"Elements"	0.07±.02	[25]
"Isotopes"	0.04±.01	[27]

where the values are from Table 2 with $\sigma_{14}/\sigma_{15} \simeq 0.57$ [15]. To achieve $(^{14}N/O)s = 0.07$ requires σ_{14}/σ_{15} to be in error by a factor of ~1.5, while $(^{14}N/O)s \geq 0.10$ (typical of the solar system and ISM) requires errors of a factor of ≥ 3 [11], which seems unlikely. Thus the isotope method is inherently much less sensitive to cross section and propagation model uncertainties, and therefore should be more accurate.

Given that the isotope results are inconsistent with $^{14}N/O \geq 0.10$, there are several possible implications:

1) Errors in the N Abundance: According to J. P. Meyer [28] uncertainties in determining the solar system and local ISM N/O ratio allow a value as low as 0.07. Coupled with cross section errors (factor of ~1.5) one might then reconcile GCRS and solar system N. However this would imply a factor of ~2 enhancement of N in solar flares (Table 3).

2) Atomic selection effects strongly favoring O over N: Always possible, but not predicted by present models.

3) ^{14}N depleted in GCR source material: The remaining possibility is significant depletion of ^{14}N in the GCR source with respect to the solar system and local ISM, as implied by the isotope method (1.2-2, 4-3). This would be inconsistent with a majority of cosmic rays originating from local ISM material [9,11] but consistent with supernova models [10].

3. The Composition of UH (Z > 30) Cosmic Rays

3.1 Observations: Although nuclei with Z>30 comprise ~2/3 of the periodic table, their abundance in nature and in cosmic rays is only $\sim 10^{-4}$ of that of Fe. These nuclei are, however, of particular interest for several reasons: a) Nuclei with Z > 30 are synthesized predominantly via the "r" and "s" neutron capture processes each of which has a characteristic elemental abundance distribution. A determination of the relative contribution of these processes to cosmic ray nuclei would provide important clues to the origin and evolution of GCR source material. Earlier studies (see, e.g., [29], [30]) have concluded that r-process nuclei dominate the Z > 70 charge spectrum, a conclusion supported by Fowler et al. [31], based on Ariel-6 data.

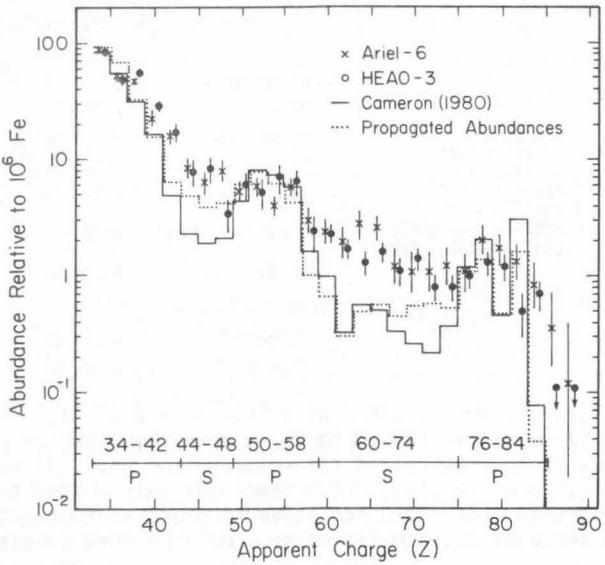

Figure 6: UH abundances in 2-charge unit bins (Fe = 10^6). The Ariel (H.2-10) and HEAO-3 (H.2-8, H.2-9, [7]) charge assignments are preliminary and assume Z^2 dependence. Corrections for resolution and for nuclear interactions in the instrument are not included. The propagated abundances assume a solar system source [8] and λ = 5.5 g/cm^2 of ISM (H.3-15). Charge groups marked P (primary) and S (secondary) are discussed in the text. The actinide region (Z≥90) is treated in Figure 10.

b) Because of their short mean free paths (~1 to 2 g/cm^2 of H), UH nuclei provide sensitive tests of cosmic ray propagation models. c) There are a number of radioactive nuclei, especially in the actinide region (Z≥90), that might serve as clocks for measuring various cosmic ray time scales.

At this conference new data were presented from the first two space-borne electronic detectors specifically designed to measure UH nuclei. These instruments, carried on Ariel-6 and HEAO-3, provide improved charge resolution over plastic and emulsion detectors used earlier in this charge region, and cover the entire charge spectrum from $Z \simeq 20$ to $Z \geq 100$.

Figure 6 shows raw charge spectra from both instruments for $34 \leq Z \leq 88$. While the charge assignments in Figure 6 are not final, and systematic corrections remain to be applied, they are probably good to a few charge units, sufficient to delineate the overall features of the spectrum.

Also shown in Figure 6 are Cameron's solar system abundances [8], and the result of propagating these abundances through a 5.5 g/cm^2 exponential pathlength distribution. Note that the four spectra share several common features, including a decreasing abundance distribution

from $Z \simeq 34$ to $Z \simeq 44$, and sudden drops in abundance just beyond $Z \simeq 56$ and $Z \simeq 84$, which argue that the assigned charge scale is not grossly in error. Further confirmation of this is seen in Figure 7, which shows a higher resolution subset of HEAO data. In the top panel, where higher order corrections are applied to the detector response, the resolution of the even-Z peaks for $30 \leq Z \leq 42$ is improved and suggestive peaks are emerging in the $50 \leq Z \leq 56$ region. Further analysis should improve the resolution and extend the energy interval covered.

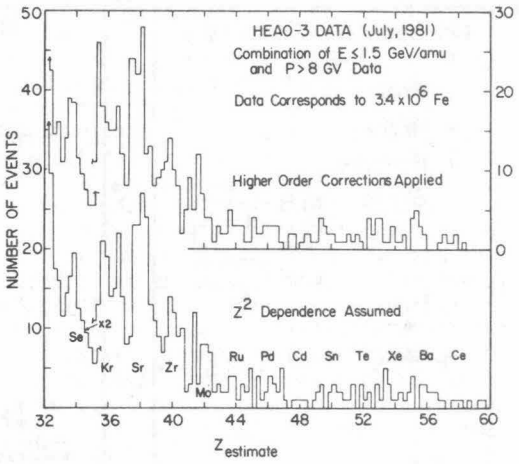

Figure 7: High-resolution subset of HEAO data. The lower scale assumes Z^2 scaling; the upper includes higher order corrections.

Using the data in Figure 7, Klarmann et al. (H.2-8, see also [6]) concluded that the source abundances of the even-Z nuclei with $30 \leq Z \leq 40$ are, in general, consistent with a solar system source (when first ionization potential effects are included; see Figure 4), but not consistent with a pure r-process source, a conclusion based mainly on the Sr abundance. These authors have not yet addressed quantitatively the question of whether the relative mix of r- and s-process material is solar-like. The extension of nucleosynthesis comparisons to higher charges ($Z > 40$) requires accurate knowledge of the charge scale, and is best addressed in terms of individual element abundances. Since the experimental situation should improve in the near future, I will focus in this report only on the general features of the charge spectrum evident in Figure 6.

3.2 Preliminary Comparison of Measured and Calculated UH Abundances:

Several new theoretical studies of UH propagation investigated the effects of: a) the pathlength distribution (H.3-9, H.3-14); b) atomic effects including first ionization potential dependence (H.3-9, H.3-12, H.3-13, H.3-14, H.3-15, H.3-16, 4-7) and c) nucleosynthesis contributions (H.3-9, H.3-12, H.3-13, H.3-16, 4-7). In this section a preliminary attempt is made to compare some of these calculations to the data.

Perhaps the most obvious difference between the calculated and observed charge spectra in Figure 6 is the extent to which the "valleys" below the abundance peaks at $Z \simeq 50$-58 and $Z \simeq 74$-84 are filled in in the two observed spectra. Fowler et al. [31] suggested that a possible explanation for their observed overabundance near $Z \simeq 64$-66 might be contributions from the fission of super-heavy nuclei. Other possible contributions are considered below.

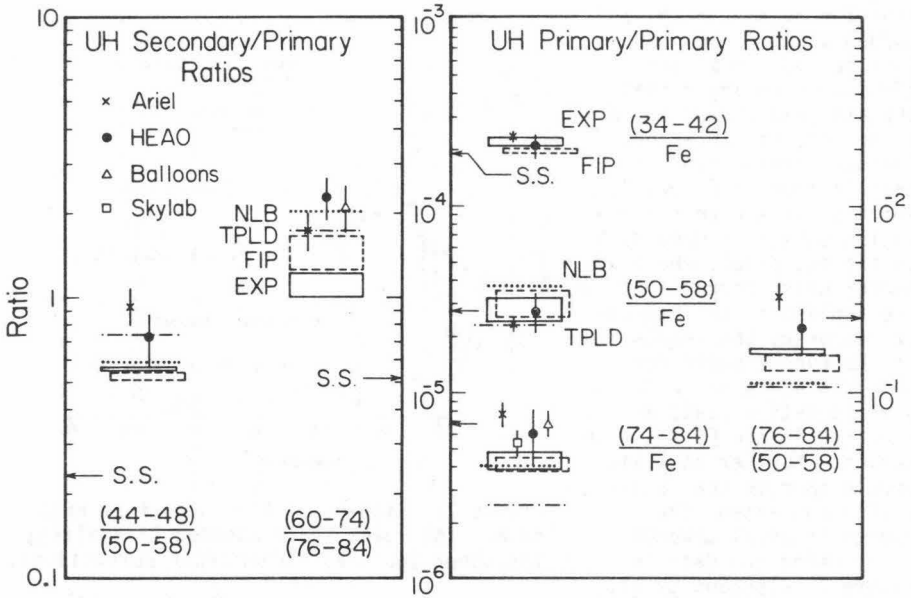

Figure 8 (left): Measured and calculated "secondary/primary" ratios. Calculated ratios are from (H.3-9, H.3-13, H.3-14, H.3-15, H.3-16) with additional results from S. H. Margolis, R.J. Protheroe, R. Silberberg, and C. J. Waddington. Pathlength distributions: —— 5 g/cm^2 exponential (EXP); --- EXP with first ionization potential (FIP) dependence; ···· nested leaky box (NLB) (H.3-9); •—• truncated pathlength distribution (TPLD) (H.3-13). NLB and TPLD include FIP effects. Boxes indicate the spread of the calculations. Arrows indicate solar system (S.S) ratios [8] used for source abundances. Data references: Ariel (H.2-10 and P. H. Fowler, priv. comm.); HEAO (H.2-8, H.2-9, and M. H. Israel, priv. comm.); Balloons [31]; Skylab [29], [31]. Both Ariel and HEAO include preliminary nuclear interaction corrections. In addition HEAO includes estimated systematic uncertainties at this (preliminary) stage of the analysis.

Figure 9 (right): Same as Figure 8 but for "primary/primary" ratios.

At an informal meeting that included the UH experimenters and the authors of the propagation studies, it was decided to compare the observed and calculated abundances in five broad charge groups (defined in Figure 6) including three groups expected to be dominated by "primary" nuclei, and two "secondary" groups where fragmentation effects should be most evident. Figures 8 and 9 summarize the results of this comparison.

Figure 8 shows two "secondary/primary" ratios which might be considered analagous to the L/M and (Fe-secondary)/Fe ratios used to

study the propagation of $6 \leq Z \leq 26$ nuclei. In both cases the observed ratios are a factor of ~4 greater than the assumed source ratios, and a factor of ~2 greater than calculated for a standard exponential path-length distribution (EXP). Note, however, that the observed excess of Z = 60-74 nuclei in Figure 8 is a factor of ~2 less than when normalized to Fe as in Figure 6. The inclusion of first ionization potential (FIP) effects improves the agreement considerably for the (60-74)/(76-84) ratio but has little effect on (44-48)/(50-58)(see H.3-9 and H.3-14). The agreement is further improved (and might be considered reasonable) for models that increase fragmentation by eliminating short pathlengths, such as the truncated pathlength distribution (TPLD) (H.3-13), and the nested-leaky-box (NLB) model (H.3-9). It therefore appears that the extent to which the UH peaks have been eroded to fill the valleys might be accounted for by a combination of FIP dependence (certainly reasonable in view of Figure 4) and somewhat greater fragmentation contributions than might be expected. These effects on the spectrum must be sorted out and determined quantitatively before it is possible to ascertain whether there are source contributions to the (44-48) or (60-74) groups due to other effects, such as that suggested in [31].

Figure 9 shows the results for four "primary/primary" ratios. Note that while the measured (34-42)/Fe and (50-58)/Fe ratios are in general agreement with the calculated values, all measurements of both the (76-84)/Fe and (76-84)/(50-58) ratios exceed the calculations (at least for the models considered here), as noted by Fowler et al. [31]. This "Pt + Pb" overabundance is magnified for the NLB and TPLD models that agree best with the secondary/primary ratios in Figure 8.

It is interesting that although the "Pt + Pb" abundance exceeds the calculations, it agrees with the source abundance before propagation (as do the other primary groups); the difference is a result of the predicted attenuation of $Z \simeq 80$ nuclei due to their large interaction cross sections. The attenuation of other primary groups (e.g., Z=50-58) is much less because they receive sizable secondary contributions from heavier nuclei (Tsao et al. H.3-16; and R. J. Protheroe, private communication). It would be difficult for a propagation model (based on a solar system source composition) to account for the secondary/primary ratios in Figure 8, and not attenuate the Z = (76-84) group with respect to lighter nuclei. It therefore appears that all available data support the conclusion [31] that the cosmic rays are enriched in Z = 76-84 nuclei with respect to the solar system by a factor of ~2. It is of course possible that either nuclear or atomic effects (other than FIP) might be the cause of such an enrichment.

Clearly UH propagation must be studied in more detail, since it has a significant effect on the derivation of source abundances for "primary" nuclei. Several other tests might be suggested. Figure 2 of (H.3-9) suggests that secondary contributions will vary with energy by an amount that should be measurable in subsets of the Ariel and HEAO data. Secondly, somewhat more restricted charge groups may be more sensitive to secondary contributions, but less sensitive to FIP effects (e.g. $68 \leq Z \leq 72$). Ultimately one would like to test the model calculations against the abundances of individual nuclei (at least even-Z, if not odd-Z). Finally, an effort should be made to reconcile propagation models for UH nuclei with observations of $Z \leq 30$ nuclei.

3.3 The Cosmic Ray Actinide Abundance: Earlier UH observations made using Lexan track detectors and nuclear emulsions have reported an overabundance of "actinides" ($Z \geq 90$ nuclei) in cosmic rays relative to solar system abundances (e.g., [32], [29], but see also [33]), a result which has supported the view that UH cosmic rays are dominated by r-process nucleosynthesis products (see, e.g., [30]).

Figure 10 summarizes reported "actinide/(Pt+Pb)" ratios. Note that both Ariel and HEAO measure a significantly lower actinide abundance than was found in either the balloon or Skylab data, although Price [34] has pointed out that a high energy subset of the Skylab data is consistent with the new results. With this exception, the Ariel and HEAO data are consistent with the broad features and flux levels of the UH charge spectrum measured by the earlier experiments (see Figures 8 and 9).

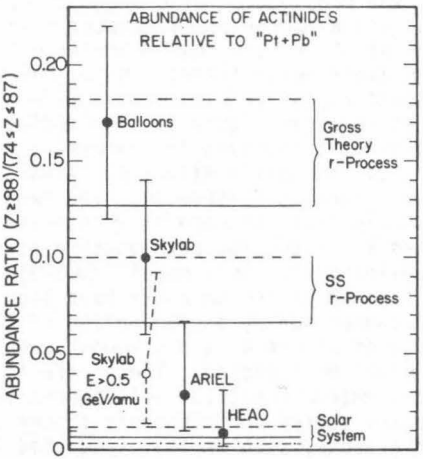

Figure 10: Measured and calculated Actinide/"Pt+Pb" ratios (from [7]) including earlier balloon [32] and Skylab [29] results. The calculations are from [30]. The dashed line includes FIP effects. The dot-dash line [35] assumes a present-day solar system source.

Combining the Ariel (2 actinides, 69 "Pt+Pb") and HEAO (1 actinide, 106 "Pt+Pb") data, we get a best estimate of 3/175 = 0.017(+.017,-.009) for this ratio. This result is not consistent with the calculated values for a pure r-process source, but is consistent with calculations based on a solar system source composition [7]. Considering both the experimental and theoretical uncertainties, this comparison still allows for the possibility that r-process nuclei could be enhanced in cosmic rays by several times over their solar system abundance.

4. Cosmic Ray Clocks - The ^{54}Mn Problem

Since this conference included the first quantitative attempt to exploit ^{54}Mn as a clock, I will spend some time discussing its interpretation. Of the Mn isotopes, ^{55}Mn is stable, while ^{53}Mn and ^{54}Mn normally decay by electron capture with half-lives of 3.7×10^6 yr. and 312 days, respectively. In high energy cosmic rays ^{53}Mn and ^{54}Mn can be considered stable against electron capture [36], but ^{54}Mn may also β-decay with an estimated half-life of $\sim 2 \times 10^6$ yr. [37], a value that may be uncertain by an order of magnitude. Cassé [37] has suggested that ^{54}Mn, a product of Fe fragmentation, might serve as a clock analogous to ^{10}Be, and thereby test whether Fe-group and CNO nuclei have had a similar propagation history.

In (H.3-2) Koch et al. presented the first high precision measurements of the Mn/Fe ratio over an extended energy interval (see Figure 11). They found that Mn has a significantly flatter energy spectrum than other

Fe fragments such as Sc, Ti, V, and Cr, and concluded that the Mn/Fe ratio is best explained by energy-dependent decay of ^{54}Mn, with the product $n_H T \simeq 0.3$ Myr.cm^{-3}, where n_H is the average density (cm^{-3}) of the confinement region, and T is the ^{54}Mn beta-decay lifetime in units of 10^6 yr. In this case the calculated surviving fraction of ^{54}Mn varies from ~50% at 1 GeV/nucleon to ~85% at 15 GeV/nuc.

A second interpretation of this problem was presented by Ormes and Protheroe (H.3-7 and revised calculations presented during their talk) who concluded that the same data could be fit assuming all ^{54}Mn survives. The essential difference between these two studies is the cross sections used. Ormes and Protheroe used semi-empirical cross sections [38] for Fe → Sc to Mn, while Koch et al. adopted cross sections based on a combination of measured and semi-empirical values, some of which (Ti, V, Cr) were then (to some extent arbitrarily) "modified" by factors up to ~20% in order to achieve better agreement with the cosmic ray observations (see H.3-6).

The Mn/Fe ratio in Figure 11 is a product of several factors, including the pathlength, the total interaction cross section of Fe, the Mn production cross sections, and ^{54}Mn decay, all of which vary with energy. Another approach to this problem is through the ratio Mn/(Sc+Ti+V+Cr), essentially a "secondary/secondary" ratio. This approach has the advantage that it cancels the effects of two energy dependent

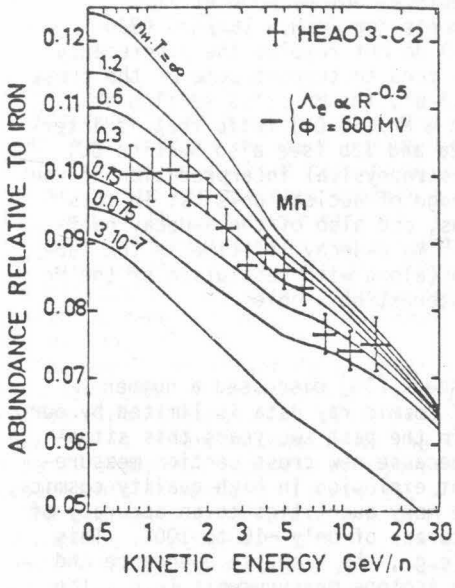

Figure 11: The Mn/Fe ratio from H.3-2. The calculated curves are parameterized by $n_H T$, where n_H is the density (cm^{-3}) and T the ^{54}Mn half-life (units of 10^6 years).

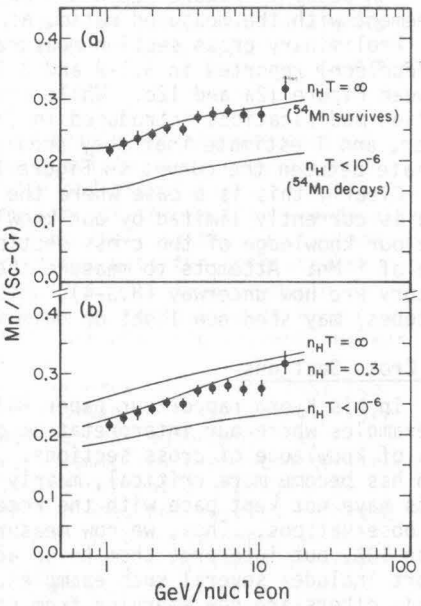

Figure 12: The Mn/(Sc+Ti+V+Cr) ratio. Observations: H.3-2. Calculations: a) H.3-7 and priv. comm.; b) H.3-6. Both assume a solar source for Sc to Fe.

parameters (the pathlength and total interaction cross section), leaving essentially a ratio of relative production cross sections, and ^{54}Mn decay (see also [37]). Figure 12 shows the observations of this ratio, and the predictions from the two studies. While the Ormes and Protheroe curves (Figure 12a) provide an excellent fit to the data assuming complete ^{54}Mn survival, this agreement may be somewhat fortuitous in that the predicted abundances of Sc to Cr individually are not in complete agreement with the data.

Figure 12b compares the predictions of Koch et al. (derived from H.3-2) to the data. In this case $n_H T = 0.3$ does provide an acceptable fit, and if the cross sections used are accurate, one must conclude that a good fraction, but not all, of ^{54}Mn has decayed. Note, however, that the fact that ^{54}Mn has a flatter energy spectrum than Sc-Cr does not in itself imply that the ^{54}Mn survival fraction is energy dependent (see also H.3-7). In both Figures 12a and 12b the curves for ^{54}Mn survival also increase with energy, as a result only of the energy dependent production cross sections. Indeed, if the relative cross sections used in Figure 12b were in error by a constant factor of ~10-15% (not, in my opinion, inconsistent with the available cross section measurements), the curve for ^{54}Mn survival could be lowered to be in excellent agreement with the data. Alternatively, if the Mn source abundance were increased by a factor of ~3 over its solar system value (Mn/Fe ≃ 0.010), the curve for ^{54}Mn decay in Figure 12b would be raised, and brought into reasonable agreement with the measured ratio, as pointed out by Koch et al.

Preliminary cross section measurements for Fe+H → $16 \leq \overline{Z} \leq 25$ (800 MeV/nucleon) reported in 3.1-2 and 3.1-3 do not resolve the discrepancy between Figure 12a and 12b. While they tend to support some of the cross section modifications introduced in (H.3-6), the Mn cross section is lower, and I estimate that they predict a Mn/(Sc-Cr) ratio that is intermediate between the curves in Figure 12a and 12b (see also Section 5.)

Clearly this is a case where the astrophysical interpretation of the data is currently limited by our knowledge of nuclear physics; in this case our knowledge of the cross sections, and also of the β-decay half-life of ^{54}Mn. Attempts to measure the ^{54}Mn β-decay lifetime in the laboratory are now underway (H.3-4), which (along with resolution of the Mn isotopes) may shed new light on this interesting problem.

5. Cross Sections

In his Kyoto rapporteur paper Raisbeck [39] discussed a number of examples where our interpretation of cosmic ray data is limited by our lack of knowledge of cross sections. In the past two years this situation has become more critical, mainly because new cross section measurements have not kept pace with the recent explosion in high quality cosmic ray observations. Thus, we now measure many quantities to an accuracy of ~1 to 10%, but interpret them to an accuracy of only ~10 to 100%. This report includes several such examples (e.g., the N source abundance and ^{54}Mn); others are now emerging from new isotope measurements (e.g., the ^{13}C and ^{18}O source abundances; see Section 6).

Fortunately, there is evidence of progress in this area, including the work of the New Hampshire (3.1-2, 3.1-3) and the Minnesota (3.1-1) groups, who reported results from two Bevalac experiments on Fe fragmentation. Paper (3.1-3) reported preliminary cross sections for isotope

production (~800 MeV/nucleon) on a hydrogen target (CH_2-C subtraction). One significant observation was that the scaling factor from heavy nuclei targets to a H target depends on both beam energy and the charge of the fragment, contrary to the usual assumption made, for example, in performing atmospheric corrections for balloon experiments.

Comparing the preliminary isotope cross sections from (3.1-3) to earlier 600 MeV/nucleon measurements by Perron [40], or to semi-empirical values [38] (not independent from [40]), I noted some systematic differences. The ratio of (3.1-3) to [40] for V, Cr, and Mn depends smoothly on the fragment neutron excess; it is ~0.3 to 0.8 for the neutron-deficient fragments, and up to ~4 for the neutron-rich fragments. Although the differences are greatest for the smallest cross sections, such experimental discrepancies should be examined before new measurements are implemented in propagation calculations.

On a related topic, Freier (3.1-5) reported on the "Cosmic Ray Sweepstakes", a comparison of propagation codes for a standard problem worked by nine different groups. All participants were "winners", as the exercise proved successful in exposing errors in cross section implementation, and in characterizing the level of agreement/disagreement (~10%) between different approaches to a common problem. Differences of the same magnitude occur in the UH calculations in Figures 8 and 9. Thus systematic "uncertainties" in our propagation codes (independent of cross sections) in many cases now exceed the observational uncertainties (at least for $Z \leq 28$). The activities of this informal group are continuing with a current focus on obtaining updated cross section data.

6. Cosmic Ray Isotopes

Although it is only recently that high-resolution measurements of cosmic ray isotopes became experimentally possible, they have already altered our views of both cosmic ray origin and propagation. This is because cosmic ray isotopes contain a new kind of information - a detailed record of their nuclear history, including their synthesis in stars and subsequent high-energy nuclear interactions with the interstellar gas. The cosmic ray element distribution, in contrast, appears to be determined mainly by atomic interactions, and it reflects only very weakly the rare isotopic species that carry the most significant nuclear information.

The most significant developments in this area during the last two years have come in determining the source abundances of relatively rare neutron-rich isotopes. At Kyoto there was general agreement that $^{22}Ne/^{20}Ne$ is enhanced, making Ne the first cosmic ray element determined to be of anomalous isotopic composition. The current status of ^{22}Ne measurements is shown in Figure 13, which includes new results reported by New Hampshire (4-3) and a preliminary mean mass measurement at ~2.5 GeV/nucleon by HEAO3-C2 (H.2-3). In essentially all of these observations $^{22}Ne/^{20}Ne$ is substantially greater than expected from a source composed of either Neon-A or solar wind neon, the two most likely possibilities for the solar composition. After correction for secondary contributions, the cosmic ray source $^{22}Ne/^{20}Ne$ ratio is a factor of 3 to 4 greater than in Neon-A and solar flare neon ([41], [42]), and a factor of 5 to 6 greater than in solar wind neon (or Neon-B). There is presently no evidence for an energy dependence in this enhancement factor.

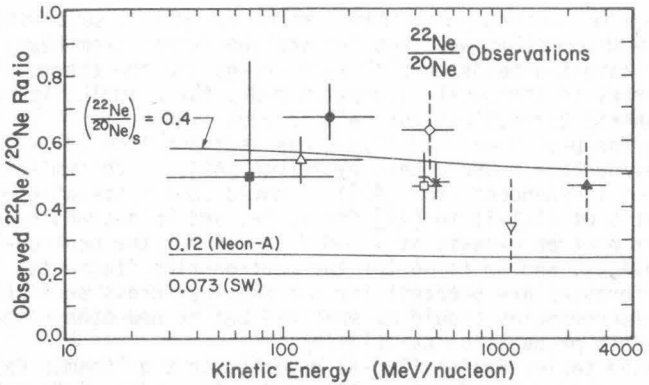

Figure 13: Measured and calculated $^{22}Ne/^{20}Ne$ ratios. The calculated curves [43] assume λ=6 g/cm^2 and three possible source compositions, including neon-A and solar wind (SW) neon. Mean mass measurements (symbols ◇, ▽, and ▲) were converted to $^{22}Ne/^{20}Ne$ ratios assuming $^{21}Ne/Ne$ = 0.10. Solid error bars represent "resolved" isotope measurements while dashed error bars indicate "unresolved" measurements (see text). For references to the data see Figure 14.

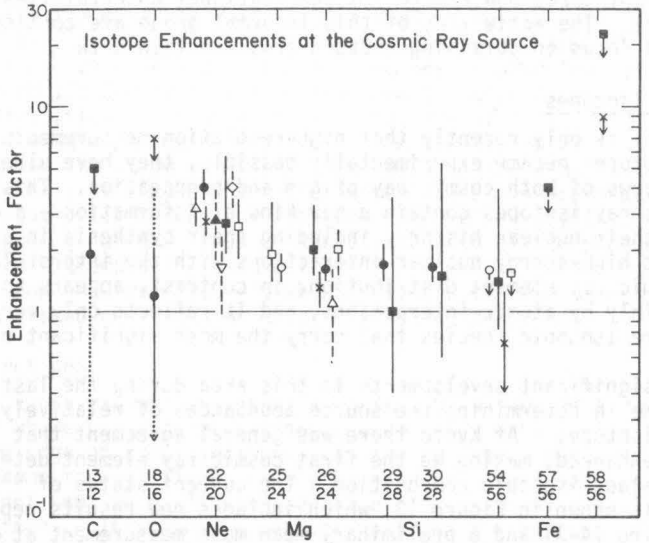

Figure 14: Cosmic ray source enhancement factors (GCR source isotope ratio divided by value in [8]) for various isotopic ratios. Dotted extensions to the C and O error bars indicate propagation uncertainties (1.2-4). Satellite data: ● Berkeley (1.2-4, [44], [45]); ■ Caltech (1.2-2, [11], [46], [47]); △ Chicago ([48], [49]); ▲ HEAO-C2 (H.2-3, [1]). Balloon data: ○ Berkeley [50]; ▽ Chicago ([16], [61], R. Dwyer, priv. comm.); ◇ Goddard [51]; □ Minnesota ([52],[53]); × New Hampshire (1.2-6), (4-3).

Figure 14 summarizes selected determinations of the source composition of other elements, compared to solar system abundances from [8]. Both Figures 13 and 14 include a distinction between "resolved" and "unresolved" isotope measurements to aid the reader in judging their possible significance. The test of resolution [54,55] was whether the mass resolution achieved was sufficient to exhibit a "valley" between adjacent isotopes in question. If so, it is likely that statistical uncertainties dominate and that the quoted error bars are realistic. In the case of "unresolved" measurements (including "mean-mass" measurements) it is possible that systematic uncertainties not reflected in the quoted error bars may dominate. Thus, greater weight should be given to "resolved" measurements, such as the Berkeley ISEE-3 data (1.2-4) in Figure 15, which shows resolved peaks at all stable isotopes, and represents the best combination of resolution and statistics achieved to date.

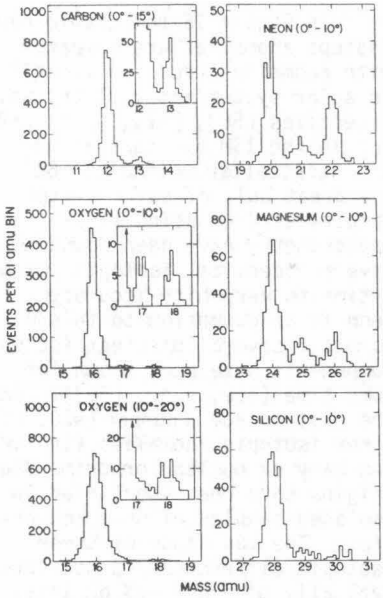

Figure 15: Mass histograms from the Berkeley ISEE-3 experiment.

Figure 14 illustrates the considerable progress that has been made in the last two years. For the Mg isotopes later measurements (in particular [44]) have confirmed the Caltech measurements [46], which found both ^{25}Mg and ^{26}Mg to be enhanced. In addition the Berkeley group also finds ^{29}Si and ^{30}Si to be enhanced by a similar factor of ~1.5 to 2 [45]. A ^{13}C enhancement is also possible, but in this case (as for ^{18}O) propagation uncertainties (mainly cross section uncertainties) dominate and preclude a definite conclusion. Note that for the other isotopes plotted, propagation uncertainties do not dominate the source determination (1.2-4). For Fe the situation isn't yet clear. It appears that ^{54}Fe cannot be enhanced by more than a factor of ~2, but large enhancements in ^{57}Fe and ^{58}Fe are still possible.

The following pattern emerges from Figure 14: There are now at least 5 cases (^{22}Ne, ^{25,26}Mg and ^{29,30}Si) where the abundances of the neutron-rich isotopes are enriched by a significant factor (~50% or more) with respect to solar system abundances. A somewhat stronger statement (paraphrased from [43]) is the following: Up to this point, all cosmic ray isotopic ratios that have been determined to ~ ±50% have been found to differ from the corresponding Cameron [8] ratio. Thus, cosmic ray isotope "anomalies" appear to be the rule, rather than the exception. Clearly it is important to see if this pattern extends to other elements. On the theoretical side, it would appear that models of cosmic ray sources should consider a pattern of several (most likely related) anomalies, not just neutron-rich Ne. (See the rapporteur paper by M. Cassé for a summary of models designed to interpret the cosmic ray source isotope composition).

In Figure 16 the cosmic ray isotope anomalies are compared with anomalies recently identified in solar system material including meteorites [56], [57], [58], [59], and in the ISM by observations of interstellar molecules [60]. The great bulk of solar system samples studied using mass-spectrometry have been found to have an identical isotopic composition to very high accuracy. Neon is an exception to this uniformity: several distinct isotopic components have been known for some time (see, e.g., [56]). In the past decade a number ($\gtrsim$20) of other isotopic anomalies (including many of nuclear or primordial origin) have been identified in isolated samples of some meteorites. The magnitude of these isotopic differences is not large, typically of order ~1% or less. By comparison, the scale of the cosmic ray anomalies, and those detected in the ISM is more like a factor of ~2. Although cosmic-ray and ISM isotope spectroscopy will perhaps never achieve the extremely high precision of the laboratory mass spectrometers used to study meteoritic material, fortunately it does not appear necessary - the magnitude of the signal is much larger.

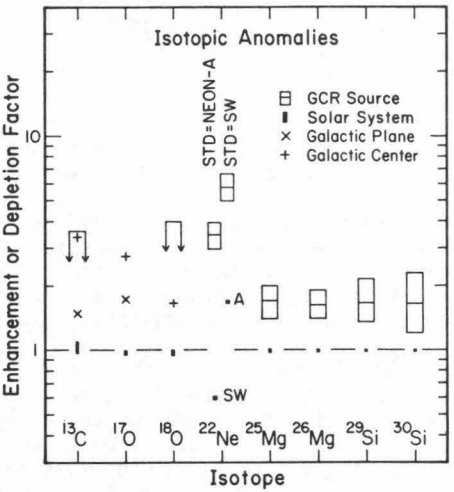

Figure 16: Isotopic anomalies in the GCRS, ISM (x,+), and solar system. An "anomaly" is a case where the isotope abundance relative to the dominant isotope (e.g. $^{26}Mg/^{24}Mg$) differs from [8]. Two possible ^{22}Ne standards are included: neon-A (A) and solar wind neon (SW). Anomalies shown are known (or likely) to be of nuclear origin, with the possible exception of solar system ^{13}C. The GCR values are weighted means of "resolved" measurements (Figure 14; propagation uncertainties included).

The most important impact of isotope anomalies is their effect on our thinking. This is illustrated by an analogy suggested to me by S. E. Woosley. Prior to the 1970's studies of solar system material emphasized its isotopic homogeneity - the high degree to which the original products of nucleosynthesis have been mixed. The discovery of a broad spectrum of meteoritic anomalies has now demonstrated that the primordial solar system was, in fact, not homogeneous, and has provided clues that are revolutionizing models of solar system origin and evolution. By analogy, cosmic ray measurements up through the end of the 1970's (with some exceptions) demonstrated the overall similarity of the elemental composition to solar system (in particular, solar flare) abundances, and showed that the isotopic abundances were also similar, at least to the extent that the same isotopes (e.g. ^{12}C, ^{16}O, ^{20}Ne, ^{24}Mg, ^{28}Si, ^{56}Fe) dominate the composition. With the development of high resolution isotope spectrometers, we are now discovering the differences - thereby revealing the heterogeneity of the galaxy. It is possible that experimental break-throughs such as these

may lead to a similar revolution in our thinking about the origin and evolution of galactic matter.

7. Summary and Conclusions

During the past two years there have been significant advances in the precision of cosmic ray measurements, as evidenced in particular by the new data from Ariel, HEAO, and ISEE. These new observations suggest that:

1) Cosmic ray elemental abundance differences from the solar system continue to be ordered by atomic parameters such as first ionization potential, at least up through Z=40. However, there appear to be important exceptions to this rule at H, He, C, N, and possibly Ne and Mo.

2) The composition of UH cosmic rays is unlike what might have been expected, suggesting that propagation effects are significant. The abundance of the "Pt-Pb" region appears to be enhanced.

3) The isotopic composition of the cosmic ray source is unlike that of the solar system, suggesting that cosmic ray "anomalies" are the rule rather than the exception. The emerging pattern of neutron-rich isotope enhancements suggests substantial differences in the evolution of cosmic ray and solar system matter.

Clearly, cosmic rays are not the same as solar system matter - they are different! Indeed, the closer we look, the more they are different.

Vive la difference!

Acknowledgements: It is a pleasure to acknowledge informative discussions of the data with many experimenters, including P.H. Fowler, M.H. Israel and L. Koch, who contributed unpublished results from their experiments. I appreciate the use of unpublished calculations provided by S. Margolis, J.F. Ormes, R.J. Protheroe, R. Silberberg, C.J. Waddington, and M.E. Wiedenbeck. E.C. Stone made a number of helpful suggestions that improved the written version of this paper. Finally, I thank the Centre National d'Etudes Spatiales and the Centre National de la Recherche Scientifique for helping to support my stay in Paris. This work was supported in part by NASA under contract NAS5-20721 and grant NGR 05-001-160.

References: For conference references see Volume 2 of the Proceedings (Volume 3 for SH papers). Some papers appear in the late paper volume.

[1]L. Koch, private communication.
[2]R. Silberberg, M.M. Shapiro and C.H. Tsao, in Spallation Nuclear Reactions and their Applications, ed. B.S.P. Shen and M. Merker (Dordrecht: Reidel), p. 49, 1976.
[3]M. Cassé and P. Goret, Ap. J. 221, 703, 1978.
[4]J.P. Meyer, 16th Int. Cosmic Ray Conf. (Kyoto) 2, 115, 1979.
[5]W.R. Webber, 14th Int. Cosmic Ray Conf. (Munich) 5, 1597, 1975.
[6]W.R. Binns, R.K. Fickle, T.L. Garrard, M.H. Israel, J. Klarmann, E.C. Stone and C.J. Waddington, Ap. J. (Letters) 247, in press, 1981.
[7]M.H. Israel, invited talk, this volume.
[8]A.G.W. Cameron, Center for Astrophysics Prepring #1357. (This compilation, based mainly on meteoritic and terrestrial measurements, is taken here as a best estimate of the solar elemental and isotopic composition).
[9]R. Silberberg, M.M. Shapiro and C.H. Tsao, 14th Int. Cosmic Ray Conf. (Munich) 2, 451, 1975.
[10]K.L. Hainebach, E.B. Norman and D.N. Schramm, Ap. J. 203, 245, 1976.

[11]R.A. Mewaldt, J.D. Spalding, E.C. Stone and R.E. Vogt, to be published in Ap. J. Letters, 1981.
[12]A.M. Prezler, J.C. Kish, J.A. Lezniak, G. Simpson and W.R. Webber, 14th Int. Cosmic Ray Conf. (Munich) 12, 4096, 1975.
[13]F.A. Hagen, A.J. Fisher and J.F. Ormes, Ap. J. 212, 262, 1977.
[14]A. Buffington, C.D. Orth and T.S. Mast, Ap. J. 226, 355, 1978.
[15]T.G. Guzik, Ap. J. 244, 695, 1981
[16]R. Dwyer, Ap. J. 224, 691, 1978.
[17]C. Bjarle, N-Y. Herrström, L. Jacobson, G. Jönsson and K. Kristiansson, 15th Int. Cosmic Ray Conf. (Plovdiv) 1, 313, 1977.
[18]M.W. Wiedenbeck, D.E. Greiner, F.S. Bieser, H.J. Crawford, H. Heckman and P.J. Lindstrom, 16th Int. Cosmic Ray Conf. (Kyoto) 1, 412, 1979.
[19]J.F. Zumberge, Caltech Ph.D. Thesis, 1981.
[20]J.E. Ross and L.H. Aller, Science 191, 1223, 1976.
[21]D.L. Lambert, M.N.R.A.S. 182, 249, 1978.
[22]D.L. McKenzie, H.R. Rugge, J.H. Underwood, and R.M. Young, Ap. J. 221, 342, 1978.
[23]W.R. Cook, E.C. Stone and R.E. Vogt, Ap. J. 238, L97, 1980.
[24]S.A. Hawley, Ap. J. 224, 417, 1978.
[25]Based on [2], [26], and Figure 3.
[26]J.A. Lezniak and W.R. Webber, Ap. J. 223, 676, 1978.
[27]Weighted mean of 10 experiments in Table 2, using [15].
[28]J.P. Meyer, private communication.
[29]E.K. Shirk and P.B. Price, Ap. J. 220, 719, 1978.
[30]J.B. Blake, K.L. Hainebach, D.N. Schramm and J.D. Anglin, Ap. J. 221, 694, 1978.
[31]P.H. Fowler, R.N.F. Walker, M.R.W. Masheder, R.T. Moses and A. Worley, Nature 291, 45, 1981.
[32]P.H. Fowler, C. Alexandre, V.M. Clapham, D.L. Henshaw, D. O'Sullivan, and A. Thompson, 15th Int. Cosmic Ray Conf. (Plovdiv) 11, 165, 1977.
[33]J.P. Meyer, 16th Int. Cosmic Ray Conf. (Kyoto) 1, 374, 1979.
[34]P.B. Price, private communication.
[35]C.J. Waddington, private communication.
[36]G.M. Raisbeck and F. Yiou, 14th Int. Cosmic Ray Conf. (Munich) 2, 502, 1975.
[37]M. Cassé, Ap. J. 180, 623, 1973.
[38]C.H. Tsao and R. Silberberg, 16th Int. Cosmic Ray Conf. (Kyoto) 2, 202, 1979.
[39]G.M. Raisbeck, 16th Int. Cosmic Ray Conf. (Kyoto) 14, 146, 1979.
[40]C. Perron, Phys. Rev. C 14, 1108, 1976.
[41]W.F. Dietrich and J.A. Simpson Ap. J. 231, L91, 1979.
[42]R.A. Mewaldt, J.D. Spalding, E.C. Stone and R.E. Vogt, Ap. J. 231, L97, 1979.
[43]M.W. Wiedenbeck, private communication.
[44]M.W. Wiedenbeck and D.E. Greiner, Phys. Rev. Lett. 46, 682, 1981.
[45]———, To be published in Ap. J. Letters, 1981.
[46]R.A. Mewaldt, J.D. Spalding, E.C. Stone, and R.E. Vogt, Ap. J. 235, L95, 1980.
[47]———, Ap. J. 236, L121, 1980.
[48]M. Garcia-Munoz, J.A. Simpson and J.P. Wefel, Ap. J. 232, L95, 1979.
[49]———, 16th Int. Cosmic Ray Conf. (Kyoto) 1, 436, 1979.
[50]G. Tarlé, S.P. Ahlen and B.G. Cartwright, Ap. J. 230, 607, 1979.
[51]R.C. Maehl, A.J. Fisher, F.A. Hagen and J.F. Ormes, Ap. J. 202, L119, 1975.
[52]P.S. Freier, J.S. Young and C.J. Waddington Ap. J. 240, L53, 1980.
[53]J.S. Young, P.S. Freier, C.J. Waddington, N.R. Brewster, and R.K. Fickle, Ap. J. 246, 1014, 1981.
[54]E.C. Stone, 13th Int. Cosmic Ray Conf. (Denver) 5, 3615, 1973.
[55]C.J. Waddington, 15th Int. Cosmic Ray Conf. (Plovdiv) 12, 168, 1977.
[56]F.A. Podosek, Ann. Rev. Astron. Astrophys. 16, 293, 1978.
[57]R.N. Clayton, Ann. Rev. Nucl. Part. Sci. 28, 501, 1978.
[58]T. Lee, Rev. Geophys. Space Sci. 17, 1591, 1979.
[59]R.H. Becker, Earth and Planetary Science Letters 50, 189, 1980.
[60]P.G. Wannier, Ann. Rev. Astron. Astrophys. 18, 399, 1980.
[61]R. Dwyer and P. Meyer, 16th Int. Cosmic Ray Conf. (Kyoto) 12, 97, 1979.